

Fig. 1 Concept of resonant compound metagrating with local symmetry-breaking for controlling the diffraction transmission through a single slit. **(a)** Schematic diagram of a subwavelength single slit surrounded by two metagratings of groove structures at the input interface, each covered by SiO₂ cladding. Each compound lattice metagrating consists of four supercells. **(b)** The supercell consists of two grooves within one period, which has mirror symmetry to its center. The metagrating with symmetric supercell supports two local eigenmodes: the SPPs mode of even symmetry and the ideal BIC mode of odd symmetry. **(c)** Symmetry-broken supercell with unchanged period (p), where the second groove is shifted along the x -direction. The lateral offset $\Delta_{L/R}$ defines the shift displacement. The local symmetry-broken metagratings support two distinct eigenmodes: the SPP mode and the quasi-BIC (QBIC) mode.

Here, we propose an alternative method to control the diffraction of light through a single metallic subwavelength slit, which is achieved by surrounding it with a compound lattice resonant metagrating [see Fig. 1(a)]. Such a metagrating structure supports two local eigenmodes: (i) a propagating SPP mode and (ii) a bound state in the continuum (BIC) mode [30–34]. A lateral offset between inner metaatoms (i.e., air grooves) is introduced to break the lattice symmetry, which makes ideal BIC degenerate to an excitable quasi-BIC mode and reduces the orthogonality of the two local eigenmodes. We will demonstrate that the lateral offset offers an additional degree of freedom for controlling subwavelength aperture diffraction, resulting in both extraordinarily enhanced transmission and extremely suppressed transmission. The mechanism is that the resonant metagrating acts as a unidirectional nanocoupler, which can efficiently convert the incident light into surface plasmon polariton (SPP), and its propagation direction depends on the lateral offset. Notably, our achieved transmission efficiency of 0.48 significantly surpasses the conventional Bethe limit $T \propto (w_0/\lambda)^4$ for subwavelength single-slit transmission [35]. This breakthrough originates from manipulating the orthogonality of two local eigenmodes, which enables a unidirectional SPP coupling mechanism. This approach fundamentally circumvents traditional diffraction limits, establishing a new paradigm for extreme light confinement in nanoscale apertures. Our findings provide a platform for advanced nanophotonic

applications, including high-efficiency optical sensors and enhanced nonlinear optical devices, paving the way for next-generation integrated photonic systems.

2 Model and results

To illustrate our idea, Fig. 1(a) presents the schematic of the considered geometry, where a single subwavelength air slit in a silver plate is surrounded by two metagratings at the input interface, each covered by SiO₂ cladding. The slit width is w_0 , the thickness of the SiO₂ layer/the silver plate is $t_1 = 250$ nm / $t_2 = 500$ nm. The metagrating is a periodic array of supercells [Fig. 1(b)] containing two grooves (i.e., two metaatoms) with identical widths of w , but different depths denoted as d_1 and d_2 , respectively. For geometric parameters, $w = 50$ nm, and $d_2 = d_1 + \Delta d$ with $\Delta d = 40$ nm and d_1 being a variable. The permittivity of SiO₂ is $\epsilon_d = 2.25$, and the permittivity of silver is $\epsilon_m = \epsilon_\infty - \omega_p^2 / [\omega(\omega + i\tau)]$ [36]. A Gaussian beam of transverse-magnetic (TM) polarization (its magnetic field solely along the y -axis) is normally incident to the entire structure, and the working frequency is $f = 550$ THz (corresponding to the wavelength of $\lambda = 545$ nm). To meet the momentum matching condition, i.e., $\beta_{\text{SPP}} = k_0 \sin \theta_{in} + mG$, the period of the supercell is set as $p = 328$ nm, where $k_0 = 2\pi f/c$, $G = 2\pi/p$, $\beta_{\text{SPP}} = k_0 \sqrt{\epsilon_d \epsilon_m / (\epsilon_d + \epsilon_m)} = 1.68k_0$ (being the wave vector of SPPs) and $m = \pm 1$ is the diffraction order.

Such compound metagratings are designed to support

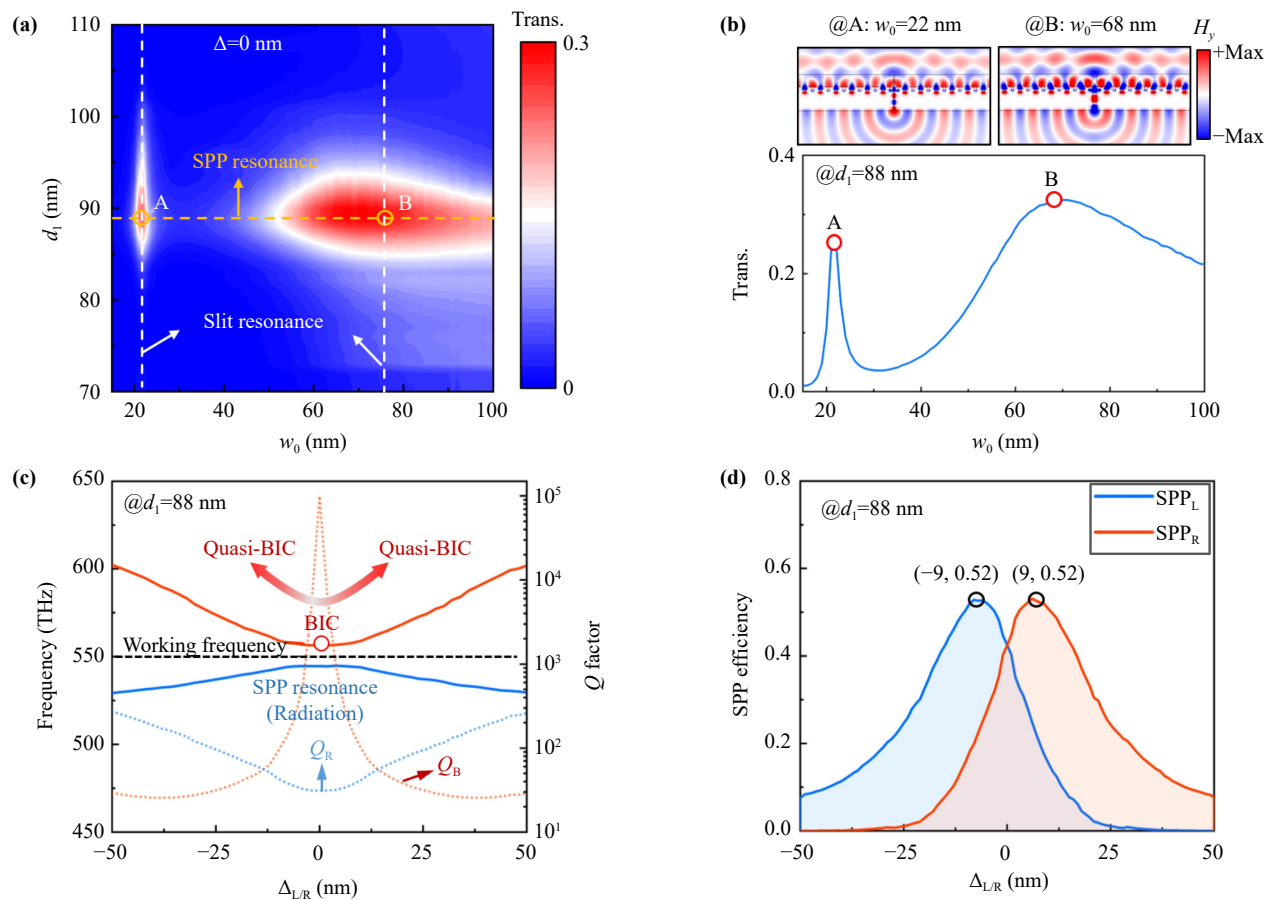


Fig. 2 The resonance modes and analysis of a subwavelength single-slit. **(a)** The subwavelength single-slit transmittance varies with the single-slit width w_0 , and the groove depth d_1 when the supercell exhibits mirror symmetry (i.e., $\Delta_{L/R} = 0$). The white dotted line represents the single-slit resonance, and the yellow curve represents the SPP resonance. Their intersection points are denoted by A and B, respectively. **(b)** At the resonance position $d_1 = 88$ nm, the transmittance of the single slit varies with the width w_0 of the single slit. The magnetic field distributions at points A and B are shown above. **(c)** At $d_1 = 88$ nm, the metagrating supports two eigenmodes: the BIC mode and the SPP resonance mode. These eigenmodes change with the lateral offset $\Delta_{L/R}$. The solid line corresponds to the eigenfrequency, while the dashed line represents the Q values associated with these two eigenmodes. **(d)** The SPP excitation efficiency on both the left and right sides of a single metagrating vs the lateral offset $\Delta_{L/R}$.

two local eigenmodes of opposite symmetry [see Fig. 1(b)]. One eigenmode is an even-symmetric SPP mode, while the other is a BIC mode with theoretically infinite quality (Q) factor [37]. The BIC mode is an odd symmetric, and cannot be excited by external incidence source. These outcomes are verified by the photonic band diagrams of the compound metagrating, as shown in Fig. 2(c) below. With the period (p) unchanged, a lateral offset $\Delta_{L/R}$ is introduced to break the mirror symmetry of the supercell, thereby transforming the ideal BIC into a quasi-BIC (QBIC). The lateral offset $\Delta_{L/R}$ represents the displacement of the second groove along the x -direction, as depicted in Fig. 1(c), where the L/R subscripts represent the left/right metagrating; $\Delta_{L/R} > 0$ defines the shift in the $+x$ direction, and $\Delta_{L/R} < 0$ is for the shift in the $-x$ direction. Due to symmetry breaking, these two local eigenmodes, which are originally

completely orthogonal, are non-orthogonal at all [see Fig. 1(c)], which can be coupled to incident light at the same time, providing a physics for the realization of unidirectional SPPs excitation.

To illustrate the diffraction transmittance of a single slit encircling by the designed structure, we first examine the case of the metagrating with $\Delta_{L/R} = 0$, where the $m = \pm 1$ order diffraction occurs for normal incidence. It implies that bidirectional SPP excitation happens in each metagrating on both sides of the single slit. Figure 2(a) displays the diffraction transmittance with two parameters of the slit width and the groove depth at the operating frequency of $f = 550$ THz. Two distinct resonance regions are observed, corresponding to two different resonance mechanisms. The first is the SPP resonance in the metagrating (indicated by the yellow dashed line), which can be adjusted by varying the

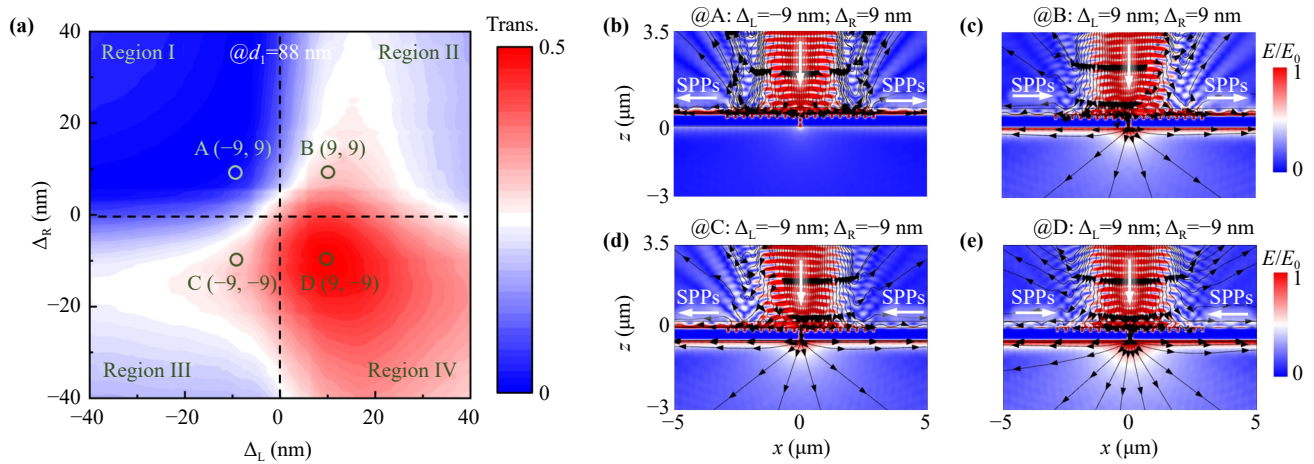


Fig. 3 Phase diagram of single-slit transmission with symmetry breaking. **(a)** Contour plot of the calculated transmittance of a subwavelength single slit versus lateral offsets Δ_L and Δ_R . **(b–e)** They correspond to the magnetic field distributions at points A, B, C, and D in the four regions shown in **(a)**. The black curves and arrows indicate the direction of energy flow. Here, $d_1 = 88$ nm, $w = 50$ nm and the single-slit width $w_0 = 68$ nm.

groove depth d_1 . The second is the FP resonance occurring within the single slit (marked by the white dashed lines), whose characteristics depend on both the width and length of the slit. The EOT effect occurs around the intersection points of these two resonances, as marked by A ($d_1 = 88$ nm & $w_0 = 22$ nm) and B ($d_1 = 88$ nm & $w_0 = 68$ nm), respectively. Figure 2(b) plots the single-slit transmittance for different slit width for $d_1 = 88$ nm. The resonance at point A exhibits a higher Q factor with a peak transmission of $T = 0.26$, whereas the resonance at point B exhibits a lower Q factor with a peak value of $T = 0.32$.

When $\Delta_{L/R} \neq 0$, the symmetry of the metagrating is broken and the BIC mode transits into QBIC mode, thereby modifying the coupling process of incident light to SPPs. Figure 2(c) illustrates the evolution of two eigenmodes (the solid curves) and their Q factors (the dashed curves) with the lateral offset $\Delta_{L/R}$. As $|\Delta_{L/R}|$ increases, the eigenfrequencies of two modes separate gradually, accompanied by an increase in the Q_R of the SPP mode and a significant decrease in the Q_B of the BIC mode. As previously mentioned, the two eigenmodes are no longer perfectly orthogonal. Consequently, the anti-symmetric QBIC mode can interfere with the symmetric SPP modes, producing asymmetric excitations of SPPs. In these calculations, the Ohmic loss of metal is ignored. Figure 2(d) shows the numerically calculated SPPs excitation efficiency vs the lateral offset $\Delta_{L/R}$, which is the ratio of the SPPs energy (at a distance of 5 μm from the center) to the incident energy. Obviously, as the lateral offset $|\Delta_{L/R}|$ increases, the efficiency of SPPs exhibits an asymmetric feature. When $\Delta_{L/R} > 0$, the excited SPPs in both metagratings predominantly propagate in the $+x$ direction. Conversely, when $\Delta_{L/R} < 0$, the excited SPPs primarily propagate in the $-x$

direction. The maximum efficiency of one-way SPPs reaches 52% when $|\Delta_{L/R}| = 9$ nm. This asymmetric SPPs propagation behavior highlights the pivotal role of the lateral offset $\Delta_{L/R}$ as a critical parameter for controlling the diffraction of light through a single slit, not just EOT effect.

Figure 3(a) shows the phase diagram of single-slit transmission as $\Delta_{L/R}$ changes, where the horizontal axis is Δ_L , while the vertical axis is Δ_R . According to their signs, the phase diagram is divided into four distinct regions. Region IV represents the enhancement region, whereas Region I, conversely, corresponds to the suppression region. In Region I, at $\Delta_L = -9$ nm and $\Delta_R = 9$ nm (i.e., point A), the diffraction transmission reaches its minimum value, i.e., $T_{\min} = 0.02$, which is caused by the fact that the excited SPPs in both metagratings propagates outward from the single slit. This result is further confirmed by the magnetic field energy flow distribution in Fig. 3(b), where the black arrows indicate the propagation direction of the energy flow. The Regions II and III are moderate regions, featured by the two excited SPPs propagating in the same direction. For a fixed Δ_R (Δ_L), increasing the lateral offset Δ_L (Δ_R) initially enhances the single-slit transmittance, followed by a subsequent decrease. This trend is consistent with the SPPs excitation efficiency as a function of lateral offset Δ_L (Δ_R) shown in Fig. 2(d). Figures 3(c) and (d) display the magnetic field distributions corresponding to point B (i.e., $\Delta_L = 9$ nm and $\Delta_R = 9$ nm) in Region II and point C (i.e., $\Delta_L = -9$ nm and $\Delta_R = -9$ nm) in Region III, respectively. In both cases, all excited SPPs propagate either to the right or the left (as indicated by white arrows), with only a portion of the energy flowing into the single slit. In Region IV, where $\Delta_L > 0$ and $\Delta_R < 0$, SPPs from both sides of metagratings propagate

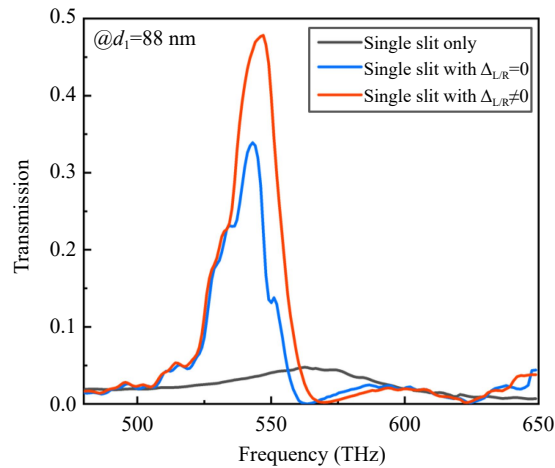


Fig. 4 Frequency response of subwavelength single-slit surrounded by two compound metagratings. The red curve is for $\Delta_L = 9$ nm and $\Delta_R = -9$ nm, the blue curve is for $\Delta_{L/R} = 0$, and the black curve is the single metallic slit only. Here, $d_1 = 88$ nm, $w = 50$ nm, and $w_0 = 68$ nm.

towards the single slit, thereby significantly enhancing the transmission of the single slit. In particular, at point D (i.e., $\Delta_L = 9$ nm and $\Delta_R = -9$ nm), the transmission reaches its maximum value, i.e., $T_{\max} = 0.48$. Figure 3(e) shows the corresponding magnetic field distribution, in which the energy flow, indicated by the black arrows, propagates towards the center, resulting in enhanced transmission.

The frequency response of the unidirectional SPPs and associated EOT effect has been explored, with obtained results as shown in Fig. 4. The red curve in Fig. 4 is for the case of the D point in the phase diagram. For comparison, the transmission spectra of both the single slit with symmetric metagrating (i.e., $\Delta_{L/R} = 0$) (the blue curve) and the single slit only (the gray curve) are presented. Compared with the case of the single slit alone, the bidirectional SPP excitations results in a narrower resonance with $Q = 26$, and the transmission efficiency is enhanced from 0.05 to 0.33 through SPPs channel coupling. Additionally, the symmetry breaking of the metagrating leads to asymmetric SPP excitations and one-way SPPs propagation, which further improves the transmission efficiency, with the maximum value reaching 0.5.

3 Conclusion

In conclusion, we have demonstrated that the compound metagrating can provide a way to control the diffraction transmission of light through a single subwavelength aperture. The compound metagrating consists of a supercell with two metaatoms, which supports two local eigenmodes of opposite symmetry, i.e., an even-symmetric SPP mode and an odd-symmetric BIC mode. We have

shown that the light diffraction of single subwavelength slit can be freely controlled by altering the inner lateral offset between the two metaatoms, producing the transmission changing from the near zero to the significantly enhanced value of about 0.5. The mechanism is that the compound metagrating can act as an efficient coupler that transforms the incident light to unidirectional propagating SPPs, and this process can be controlled by local symmetry breaking of the metagrating. The designed structure can extend to three-dimensional structures such as gradient refractive index circular plates [38]. However, due to the polarization dependence of SPPs, their propagation direction may become more diffuse, which inevitably degrades the transmission efficiency. These results are promising in many applications, such as imaging [39, 40], planar lenses [41], and sensing [42, 43].

Declarations The authors declare that they have no competing interests and there are no conflicts.

Acknowledgements This work was supported by the National Natural Science Foundation of China (Grant Nos. 12274225, 12274313 and 12274314), the Natural Science Foundation of Jiangsu Province (Grant No. BK20230089), the Collaborative Innovation Center of Suzhou Nano Science and Technology, and Suzhou Basic Research Project (No. SJC2023003), and the Gusu Leading Talent Plan for Scientific and Technological Innovation and Entrepreneurship (ZXL2024400).

References

1. C. Genet and T. W. Ebbesen, Light in tiny holes, *Nature* 445(7123), 39 (2007)
2. T. W. Ebbesen, H. J. Lezec, H. F. Ghaemi, T. Thio, and P. A. Wolff, Extraordinary optical transmission through sub-wavelength hole arrays, *Nature* 391(6668), 667 (1998)
3. L. Martín-Moreno, F. J. García-Vidal, H. J. Lezec, K. M. Pellerin, T. Thio, J. B. Pendry, and T. W. Ebbesen, Theory of extraordinary optical transmission through subwavelength hole arrays, *Phys. Rev. Lett.* 86(6), 1114 (2001)
4. F. J. Garcia-Vidal, L. Martin-Moreno, T. W. Ebbesen, and L. Kuipers, Light passing through subwavelength apertures, *Rev. Mod. Phys.* 82(1), 729 (2010)
5. H. J. Lezec, A. Degiron, E. Devaux, R. A. Linke, L. Martin-Moreno, F. J. Garcia-Vidal, and T. W. Ebbesen, Beaming light from a subwavelength aperture, *Science* 297(5582), 820 (2002)
6. H. I. Smith and M. L. Schattenburg, X-ray lithography from 500 to 30 nm: X-ray nanolithography, *IBM J. Res. Develop.* 37(3), 319 (1993)
7. E. Sharma, R. Rathi, J. Misharwal, B. Sinhmar, S. Kumari, J. Dalal, and A. Kumar, Evolution in lithography techniques: Microlithography to nanolithography, *Nanomaterials (Basel)* 12(16), 2754 (2022)
8. W. E. Moerner and D. P. Fromm, Methods of single-molecule fluorescence spectroscopy and microscopy, *Rev. Sci. Instrum.* 74(8), 3597 (2003)

9. D. Yoo, K. L. Gurunatha, H. K. Choi, D. A. Mohr, C. T. Ertsgaard, R. Gordon, and S. H. Oh, Low-power optical trapping of nanoparticles and proteins with resonant coaxial nanoaperture using 10 nm gap, *Nano Lett.* 18(6), 3637 (2018)
10. C. Chen, M. L. Juan, Y. Li, G. Maes, G. Borghs, P. Van Dorpe, and R. Quidant, Enhanced optical trapping and arrangement of nano-objects in a plasmonic nanocavity, *Nano Lett.* 12(1), 125 (2012)
11. B. Hecht, B. Sick, U. P. Wild, V. Deckert, R. Zenobi, O. J. F. Martin, and D. W. Pohl, Scanning near-field optical microscopy with aperture probes: Fundamentals and applications, *J. Chem. Phys.* 112(18), 7761 (2000)
12. B. R. Lu, C. Xu, J. Liao, J. Liu, and Y. Chen, High-resolution plasmonic structural colors from nanohole arrays with bottom metal disks, *Opt. Lett.* 41(7), 1400 (2016)
13. J. A. Porto, F. J. García-Vidal, and J. B. Pendry, Transmission resonances on metallic gratings with very narrow slits, *Phys. Rev. Lett.* 83(14), 2845 (1999)
14. D. Y. Lu, W. Li, H. Zhou, X. Cao, K. J. Wang, H. J. Luo, J. B. Li, X. M. Zhang, M. D. He, L. Xu, and J. Q. Liu, Coupling between surface plasmon polariton and planar waveguide modes in the biosensor based on metal-insulator-metal/planar waveguide structure, *Opt. Commun.* 459, 124928 (2020)
15. J. Homola, Surface plasmon resonance sensors for detection of chemical and biological species, *Chem. Rev.* 108(2), 462 (2008)
16. T. G. Mayerhöfer, R. Knipper, U. Hübner, D. Cialla-May, K. Weber, H. G. Meyer, and J. Popp, Ultra sensing by combining extraordinary optical transmission with perfect absorption, *ACS Photonics* 2(11), 1567 (2015)
17. J. N. Anker, W. P. Hall, O. Lyandres, N. C. Shah, J. Zhao, and R. P. Van Duyne, Biosensing with plasmonic nanosensors, *Nat. Mater.* 7(6), 442 (2008)
18. R. Zia, J. A. Schuller, A. Chandran, and M. L. Brongersma, Plasmonics: The next chip-scale technology, *Mater. Today* 9(7–8), 20 (2006)
19. Z. B. Li, Y. H. Yang, X. T. Kong, W. Y. Zhou, and J. G. Tian, Fabry-Pérot resonance in slit and grooves to enhance the transmission through a single subwavelength slit, *J. Opt. A* 11(10), 105002 (2009)
20. T. Thio, K. M. Pellerin, R. A. Linke, H. J. Lezec, and T. W. Ebbesen, Enhanced light transmission through a single subwavelength aperture, *Opt. Lett.* 26(24), 1972 (2001)
21. A. Degiron and T. W. Ebbesen, The role of localized surface plasmon modes in the enhanced transmission of periodic subwavelength apertures, *J. Opt. A* 7(2), S90 (2005)
22. A. Krishnan, T. Thio, T. J. Kim, H. J. Lezec, T. W. Ebbesen, P. A. Wolff, J. Pendry, L. Martin-Moreno, and F. J. Garcia-Vidal, Evanescently coupled resonance in surface plasmon enhanced transmission, *Opt. Commun.* 200(1–6), 1 (2001)
23. Z. B. Li, J. G. Tian, W. Y. Zhou, Z. B. Liu, W. P. Zang, and C. P. Zhang, Highly directional emission from a subwavelength slit in metal-dielectric layered films, *Chin. Phys. Lett.* 23(5), 1207 (2006)
24. J. Chen, Z. Li, S. Yue, J. Xiao, and Q. Gong, Plasmon-induced transparency in asymmetric T-shape single slit, *Nano Lett.* 12(5), 2494 (2012)
25. Z. Deng, Y. Cao, X. Li, and G. Wang, Multifunctional metasurface: From extraordinary optical transmission to extraordinary optical diffraction in a single structure, *Photon. Res.* 6(5), 443 (2018)
26. S. Kim, H. Kim, Y. Lim, and B. Lee, Off-axis directional beaming of optical field diffracted by a single subwavelength metal slit with asymmetric dielectric surface gratings, *Appl. Phys. Lett.* 90(5), 051113 (2007)
27. C. Chen, Y. Liu, L. Zhao, X. Hu, and Y. Fu, Asymmetric nonlinear-mode-conversion in an optical waveguide with PT symmetry, *Front. Phys. (Beijing)* 17(5), 52504 (2022)
28. S. Li, Y. Fu, L. Gao, J. H. Jiang, and Y. Xu, Controlling the light diffraction through a single subwavelength metallic slit via phase gradient, *New J. Phys.* 25(5), 053004 (2023)
29. Z. Ju, M. Deng, J. Wang, and L. Chen, Reconfigurable multifrequency and wide-angle directional beaming of light from a subwavelength metal slit with graphene metasurfaces, *Opt. Lett.* 45(10), 2882 (2020)
30. C. W. Hsu, B. Zhen, A. D. Stone, J. D. Joannopoulos, and M. Soljačić, Bound states in the continuum, *Nat. Rev. Mater.* 1(9), 16048 (2016)
31. Q. Zhou, S. Li, W. Shao, L. Gao, Y. Fu, and Y. Xu, Optical bound states in the continuum in metallic gratings with compound lattices, *Opt. Express* 32(25), 44238 (2024)
32. S. H. Fan, W. Suh, and J. D. Joannopoulos, Temporal coupled-mode theory for the Fano resonance in optical resonators, *J. Opt. Soc. Am. A* 20(3), 569 (2003)
33. S. Kim, K. H. Kim, and J. F. Cahoon, Optical bound states in the continuum with nanowire geometric superlattices, *Phys. Rev. Lett.* 122(18), 187402 (2019)
34. Q. Zhou, Y. Fu, J. Liu, H. Yan, H. Chen, L. Gao, J. Jiang, and Y. Xu, Plasmonic bound states in the continuum in compact nanostructures, *Adv. Opt. Mater.* 10(24), 2201590 (2022)
35. C. J. Bouwkamp, Diffraction theory, *Rep. Prog. Phys.* 17(1), 35 (1954)
36. S. Campione, D. De Ceglia, M. A. Vincenti, M. Scalora, and F. Capolino, Electric field enhancement in ϵ -near-zero slabs under TM-polarized oblique incidence, *Phys. Rev. B* 87(3), 035120 (2013)
37. S. I. Azzam, V. M. Shalaev, A. Boltasseva, and A. V. Kildishev, Formation of bound states in the continuum in hybrid plasmonic-photonic systems, *Phys. Rev. Lett.* 121(25), 253901 (2018)
38. X. Cui, J. Shi, X. Liu, and Y. Lai, A panel acoustic energy harvester based on the integration of acoustic metasurface and helmholtz resonator, *Appl. Phys. Lett.* 119(25), 253903 (2021)
39. L. Verslegers, P. B. Catrysse, Z. Yu, and S. Fan, Planar metallic nanoscale slit lenses for angle compensation, *Appl. Phys. Lett.* 95(7), 071112 (2009)
40. J. Lin and H. Zhang, Superresolution imaging via subwavelength hole resonances, *Phys. Rev. Appl.* 14(3), 034066 (2020)
41. L. Verslegers, P. B. Catrysse, Z. Yu, J. S. White, E. S. Barnard, M. L. Brongersma, and S. Fan, Planar lenses based on nanoscale slit arrays in a metallic film, *Nano Lett.* 9(1), 235 (2009)
42. R. Knipper, V. Jr Kopecký, U. Huebner, J. Popp, and T. G. Mayerhöfer, Slit-enhanced chiral- and broadband infrared ultra-sensing, *ACS Photonics* 5(8), 3238 (2018)
43. A. P. Blanchard-Dionne and M. Meunier, Sensing with periodic nanohole arrays, *Adv. Opt. Photonics* 9(4), 891 (2017)